

Evidence for a magnetic field-induced unconventional nematic state in the frustrated and anisotropic spin-chain cuprate LiCuSbO_4

H.-J. Grafe,¹ S. Nishimoto,^{1,2} M. Iakovleva,^{1,3} E. Vavilova,^{1,3} L. Spillecke,^{1,4} A. Alfonsov,¹ M.-I. Sturza,¹ S. Wurmehl,¹ H. Nojiri,⁵ H. Rosner,⁶ J. Richter,⁷ U.K. Rößler,¹ S.-L. Drechsler,¹ V. Kataev,^{1,*} and B. Büchner^{1,4}

¹Leibniz Institute for Solid State and Materials Research IFW-Dresden, D-01171 Dresden, Germany

²Institute for Theoretical Physics, Technical University Dresden, D-01069 Dresden, Germany

³Zavoisky Physical-Technical Institute of the Russian Academy of Sciences, 420029 Kazan, Russia

⁴Institute for Solid State Physics, Technical University Dresden, D-01069 Dresden, Germany

⁵Institute of Materials Research, Tohoku University, 980-8577, Sendai, Japan

⁶Max-Planck-Institute for Chemical Physics of Solids, Dresden, Germany

⁷Universität Magdeburg, Institut für Theoretische Physik, Germany

(Dated: September 8, 2018)

Modern theories of quantum magnetism predict exotic multipolar states in weakly interacting strongly frustrated spin-1/2 Heisenberg chains with ferromagnetic nearest neighbor (NN) inchain exchange in high magnetic fields. Experimentally these states remained elusive so far. Here we report the evidence for a long-sought magnetic field-induced nematic state arising above a field of ~ 13 T in the edge-sharing chain cuprate $\text{LiSbCuO}_4 \equiv \text{LiCuSbO}_4$. This interpretation is based on the observation of a field induced spin-gap in the measurements of the ^7Li NMR spin relaxation rate T_1^{-1} as well as a contrasting field-dependent power-law behavior of T_1^{-1} vs. T and is further supported by static magnetization and ESR data. An underlying theoretical microscopic approach favoring a nematic scenario is based essentially on the NN XYZ exchange anisotropy within a model for frustrated spin-1/2 chains. It is investigated by the DMRG technique. The employed exchange parameters are justified qualitatively by electronic structure calculations for LiCuSbO_4 .

Strong electronic correlations in solids may give rise to novel ground states of matter such as electronic liquid crystal phases in correlated metals or spin liquid states in insulating quantum magnets [1, 2]. Theory predicts that in the latter systems conventional long-range magnetic dipolar order can be suppressed down to $T = 0$ due to frustration of magnetic interactions and/or quantum fluctuations (for a review see, e.g., [3]). Though individual spins remain non-ordered in the spin liquid, higher rank magnetic multipoles (quadrupoles, octupoles etc.) can order under favorable conditions [4]. Such an exotic multipolar (MP) order does not break the time-reversal symmetry and is often referred to as a "hidden order" since it is difficult to detect experimentally by most of the available techniques sensitive to magnetic dipole moments, only. However, the spin rotational symmetry is broken in this hidden phase which is therefore also called a spin-nematic state in the simplest quadrupolar case, in analogy with the nematic order in liquid crystals, where the translational crystalline order is absent but the rotational symmetry is broken.

A prominent example of a spin liquid is a single Heisenberg spin-1/2 chain with the nearest neighbor (NN) antiferromagnetic (AFM) interaction whose ground state is described by the so-called gapless Tomonaga-Luttinger (TL) spin liquid [5]. Further complexity can be brought in the problem by including an AFM next-nearest neighbor (NNN) interaction J_2 . Irrespective of the sign of the NN coupling J_1 , AFM J_2 causes spin frustration and

may yield different phases depending on the frustration ratio $\alpha = |J_2/J_1|$ [6–8]. In particular, pioneering theoretical works [8–16] devoted mainly to one-dimensional (1D) isotropic frustrated $J_1(\text{FM}) - J_2(\text{AFM})$ chain models have predicted unusual field-induced MP states near the saturation field H_{sat} above which at $T = 0$ all spins are aligned by an external magnetic field H . These states form a TL-liquid of multiple p -bound states of magnons corresponding to nematic, triatic, quartic MP phases ($p = 2, 3, 4, \dots$). For interacting chains within 2D or 3D arrangements, the MP phases strongly compete with collinear longitudinal H -dependent incommensurate spin density wave (SDW_p) phases predominant at lower fields [17]. (Here the index p indicates the neighboring MP state.) Albeit MP phases might coexist with *non-collinear* strongly fluctuating dipolar states [18].

Low-D spin networks can be found in 3D transition metal (TM) oxides. A specific geometry of the chemical bonds can yield chains of TM ions magnetically coupled mainly via oxygen ligands in one direction. A sizable and still increasing number of frustrated CuO_2 spin-1/2 chain compounds is currently available. Nevertheless, the very existence of an MP state is not yet proved. Also the possibility of a coexistence of an MP state (and even of an ordered phase) with some other dipolar magnetic phases or corresponding strong fluctuations of them remains unclear up to now. The quest for MP phases focussed in the last years mainly on two compounds, namely LiCuVO_4 [19–21] and $\text{PbCuSO}_4(\text{OH})_2$ (linarite) [22]. Both materials exhibit at ambient fields a 3D-non-collinear spiral type dipolar order at low T due to residual interchain couplings. Various field-induced collinear SDW_p phases were detected but the theoretically proposed neighbor-

* Corresponding author: v.kataev@ifw-dresden.de

ing MP phases at higher fields remain elusive. In particular, in the case of LiCuVO_4 it was concluded that the spin-nematic phase, if it exists at all, could be established only in a very narrow field range of 1 T below $\mu_0 H_{\text{sat}} \approx 41.4 \text{ T}$ [20, 23]. Indeed, from the theoretical side it has become clear that the interchain coupling that causes dipolar magnetic order can easily destroy fragile MP phases whereas easy-axis exchange anisotropy may stabilize them [24, 25]. In this context the recent synthesis and the first physical study of a novel member of the frustrated CuO_2 -chain family, the strongly frustrated $J_1(\text{FM}) - J_2(\text{AFM})$ quasi-1D compound LiCuSbO_4 (Fig. 1), is noteworthy [26, 27]. It exhibits short-range incommensurate spin correlations below $T \sim 9 \text{ K}$ but, in contrast to the spiral spin-chain compounds LiCuVO_4 and LiCuZrO_4 [28, 29], do not show long-range magnetic order at $H = 0$ down to $T \sim 0.1 \text{ K}$. This points to a very weak or specific interchain coupling in LiCuSbO_4 . Moreover, a sizeable exchange anisotropy was estimated here, too.

Here we report the results of ^7Li NMR relaxation rate T_1^{-1} measurements in LiCuSbO_4 in a broad field range of 3 – 16 T. A surprising contrasting behavior of T_1^{-1} vs. T is observed around a special crossover field $H_{c1} \approx 13 \text{ T}$ within a rather narrow field range. At $H < H_{c1}$, $T_1^{-1}(T)$ exhibits a diverging power-law behavior suggesting a static magnetic order at lower temperatures. In contrast, in higher magnetic fields $H > H_{c1}$, $T_1^{-1}(T)$ turns into an exponential decrease indicative of the opening of a spin gap above the narrow crossover high-field region. Our analysis of the static magnetization and ESR data rules out saturation of the magnetization or Dzyaloshinskii-Moriya (DM) couplings as possible conventional reasons for the opening of this spin gap. We argue that this gap should be considered as one of the signatures of a distinctive but nevertheless naturally "hidden" for a dipolar sensitive probe MP state. In particular, we argue that such a peculiar behavior of T_1^{-1} is due to the occurrence of a dipolar spin-liquid state confined to a certain field range below H_{c1} which crosses over to the competing anisotropic spin-nematic liquid state which is stabilized above H_{c1} . Our theoretical analysis employing the density matrix renormalization group (DMRG) technique indeed reveals a broad stability region of an unconventional spin-nematic state in LiCuSbO_4 setting in above $\sim 13 \text{ T}$ and extending to $H \gtrsim 20 \text{ T}$. Altogether, our experimental observations and model calculations provide strong arguments to identify a long-sought nematic state in LiCuSbO_4 and stress the importance of anisotropic exchange for its relevance.

Results

Magnetization measurements. The T -dependence of the static magnetic susceptibility $\chi(T) = M/H$ of LiCuSbO_4 measured at a field $\mu_0 H = 3 \text{ T}$ is shown in Fig. 2. It appears to be in accord with the data of Ref. [26]. In particular, a characteristic maximum of

$\chi(T)$ is observed at $\sim 9 \text{ K}$. The dependence of the static magnetization M on the magnetic field H measured in pulsed fields up to 20 T at a low $T = 0.45 \text{ K}$ is shown in Fig. 3(a). The $M(H)$ curve exhibits a characteristic S -shape. At fields below $\sim 6 \text{ T}$ M increases almost linearly and develops an upward curvature at higher fields as expected for a simple isotropic 1D-chain [30]. However, by approaching $\sim 12 \text{ T}$ the $M(H)$ dependence

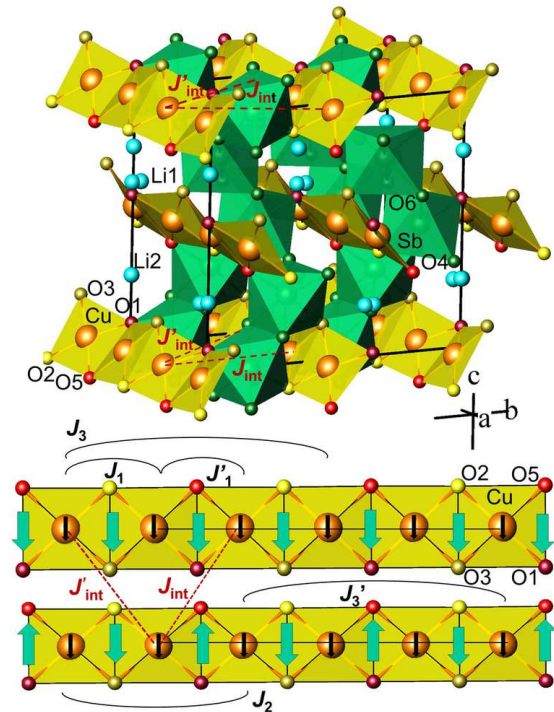


FIG. 1. Top: crystallographic structure of $\text{LiSbCuO}_4 \equiv \text{LiCuSbO}_4$ [27]. Cu^{2+} ions (orange) are bonded covalently to four nonequivalent O^{2-} ligands and form buckled non-planar CuO_4 plaquettes. Edge-shared CuO_4 plaquettes form non-ideal alternately tilted stacks (along the c -axis) of CuO_2 chains (colored yellow and brown, respectively) running along the a -axis. The chains are interconnected with SbO_6 octahedra shown in blue-green. The Li^+ ions (bright blue balls) occupy two positions. The split Li1 position is shown with overlapping balls. Bottom: Schematic view of two neighboring individual CuO_2 chains within the ab -plane ignoring their tilting and buckling (cf. Top). The relevant intrachain exchange paths are indicated by black arcs. The four nonequivalent O^{2-} ions within a CuO_4 -plaquette give rise to different left and right Cu-Cu bonds along the a -axis causing this way an *alternated* (J_1, J_1')- J_2 spin chain with small nonequivalent third neighbor couplings (J_3, J_3'). Black arrows denote the magnetically active spins and bright blue arrows the DM vectors that are confined to the (bc) -plane \perp to the chain axis whereas their mutual orientation can be arbitrary. For illustration the two limiting configurations, uniform and staggered are depicted that have been studied theoretically in single-chain approximation (Fig. 8). Dark dashed line: the frustrated weak interchain couplings J_{int} and $J'_{\text{int}} \sim 1 \text{ K} \ll J_2 < |J_1|, |J_1'|$ in the basal (ab)-plane (see also Top).

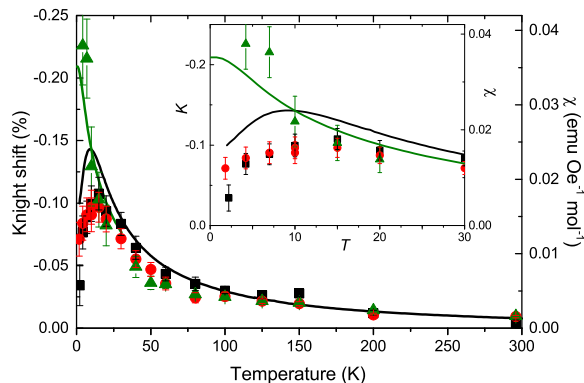


FIG. 2. Scaling of Knight shift ($K(3\text{T})$ ■, $K(9\text{T})$ ●, and $K(15\text{T})$ ▲) and macroscopic susceptibility ($\chi(3\text{T})$ —, $\chi(16\text{T})$ —). The susceptibility at 16 Tesla has been reproduced from Dutton *et al.* [26].

weakens but surprisingly *no* saturation is observed up to the highest field of 20 T. Such a peculiar $M(H)$ dependence appears to be a remarkable feature of LiCuSbO_4 as discussed in detail below [31].

ESR measurements. High-field ESR spectra of LiCuSbO_4 at all measured frequencies at temperatures $T > 20\text{K}$ consist of a symmetrical single line with the shape close to a Lorentzian [Figs. 3(b) and (c)]. Considering the polycrystalline form of our samples, this suggests that the anisotropy of the g -factor, which otherwise produces a characteristic asymmetric pattern of the spectrum [32], is smaller than the width of the signal. The g -factor of 2.18 obtained from the slope of the $\nu(H)$ dependence $g = (h/\mu_B)\nu/H$ [Fig. 3(d)] is a typical powder-averaged value for a Cu^{2+} ion in a distorted octahedral ligand coordination [33]. At $\nu = 95\text{GHz}$ which corresponds to the resonance field $\mu_0 H_{\text{res}} \approx 3.1\text{T}$ the signal remains practically a single line down to the lowest temperature. At $T \lesssim 20\text{K}$ it merely exhibits a rather small shift to smaller fields and slightly broadens, but shows no indication of an onset of a static magnetic ordering. In contrast, at $\nu \geq 270\text{GHz}$ and $\mu_0 H_{\text{res}} \geq 8.8\text{T}$ the satellite peaks P1 and P3 begin to develop besides the central peak P2 at $T \lesssim 20\text{K}$ [Figs. 3(c) and (d)]. Their offset of $\sim 0.8 - 1\text{T}$ from the main peak remains practically constant, whereas the intensity increases with increasing ν (and H) and decreasing T . The frequency vs. field dependence of P1 and P3 approximately follows the relation $\nu_{1,3} = \Delta_{1,3} + (\mu_B/h)gH$ with $\Delta_1 \approx 35\text{GHz}$ and $\Delta_3 \approx -27\text{GHz}$.

NMR measurements. Frequency swept ^7Li NMR spectra in a field of 3, 9, and 15 Tesla are shown in Fig. 4 (see methods). The width of the spectra (square root of the second moment) in 3 T and at 296 K is 26.5 kHz, indicating that any quadrupolar broadening or splitting must be significantly smaller than this value. Therefore, the shape of the powder pattern is solely determined by the anisotropic dipolar hyperfine coupling of the two dif-

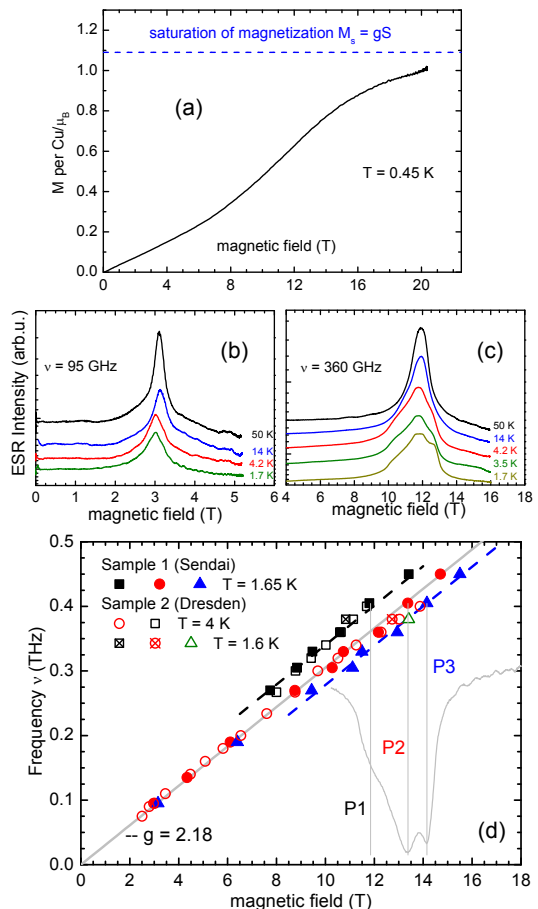


FIG. 3. Field dependence of the magnetization at $T = 0.45\text{K}$ (a). Selected ESR spectra at different temperatures at frequencies $\nu = 95\text{GHz}$ (b), and $\nu = 360\text{GHz}$ (c), and a summary of the frequency vs. field dependence of the ESR peaks at a low T plotted together with a spectrum at $\nu = 405\text{GHz}$ (d). Note the satellite peaks in the spectra in panel (c) that develop at $T < 20\text{K}$. In (d), symbols - experimental peak positions P1, P2 and P3, solid and dashed lines are linear fits. The main peak P2 follows a linear gapless branch $\nu_2 = (\mu_B/h)gH$ with $g = 2.18$, whereas the satellite branches P1 and P3 $\nu_{1,3} = \Delta_{1,3} + (\mu_B/h)gH$ exhibit offsets $\Delta_1 \approx 35\text{GHz}$ and $\Delta_3 \approx -27\text{GHz}$. (see the text)

ferent Li sites in LiCuSbO_4 times the susceptibility in the paramagnetic state. The width of the spectra scales perfectly linear with the magnetic field, indicating that the broadening of the spectra is entirely of magnetic origin. The scaling holds also at low temperatures, evidencing the absence of magnetic ordering in all fields down to $\sim 2\text{K}$. The dipolar hyperfine coupling tensor has been obtained by lattice sum calculation and is given in the Supplement.

The Knight shift, K , has been extracted from the maximum of the spectra. According to the calculated dipolar hyperfine coupling tensor, both Li sites contribute to the maximum with different elements of the tensor. K is plotted together with the macroscopic susceptibility, in Fig. 2. The scaling of the Knight shift with χ , i.e.,

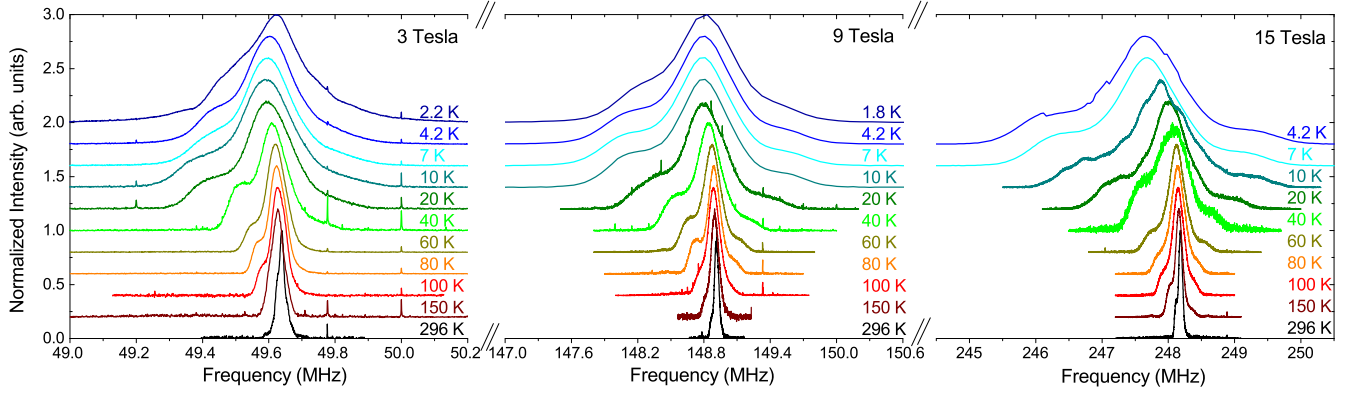


FIG. 4. NMR spectra at 3, 9 and 15 Tesla. Note that the width of the x -axis is scaled by a factor 9/3 and 15/3 for 9 and 15 Tesla with respect to the x -axis of the 3 Tesla spectra. This way, this figure shows that the broadening is paramagnetic, and that there is no magnetic order down to ~ 2 K in any field.

$K = A_{hyp} \cdot \chi$, is good down to ~ 15 K. Below 15 K, the K shows qualitatively the same T -dependence as but the error bars of K become large at low temperatures due to the strong magnetic broadening. However, the similar T -dependencies indicates that both, K and χ , are dominated by the intrinsic susceptibility and that impurity contributions are small.

The results of the measurements of the ${}^7\text{Li}$ nuclear spin-lattice relaxation rate T_1^{-1} are shown in Fig. 5. In Fig. 5(a) T_1^{-1} vs. temperature is plotted on a log-log scale for six different fields from 3 to 16 Tesla. At high T , T_1^{-1} is almost constant and field-independent as expected for a 1D spin system. However, at low T , below ~ 30 K, a dramatic field dependence develops, resulting in a difference of almost three orders of magnitude between 3 and 16 T at the lowest temperatures. For low fields below 12 T (Fig. 5(b)), T_1^{-1} diverges at low temperatures (for 3 T, T_1^{-1} increases below 7 K, for 9 and 12 T, T_1^{-1} increases already below 15 K). In contrast, for fields above 13.5 T, T_1^{-1} decreases almost exponentially at low T . This is highlighted in Figs. 5(c,d), where T_1^{-1} is plotted vs. the inverse temperature T^{-1} .

Discussion

Experiment. The central experimental result of this work is an observation of distinct temperature and magnetic field dependences of the ${}^7\text{Li}$ NMR relaxation rate T_1^{-1} in the short-range ordered (SRO) state of LiCuSbO_4 below ~ 10 K, as shown in Fig. 5, which will be discussed in the following.

NMR relaxation in magnetic solids. In magnetic materials, the nuclear spin lattice relaxation rate, T_1^{-1} , is typically caused by the transverse (i.e. \perp to the nuclear spin quantization axis) components of the time-dependent fluctuating field exerted on the nuclei by the electron spin system. It can be expressed in terms of the Fourier transforms $S^{z,\pm}(q, \omega)$ of the time-dependent longitudinal and transverse spin-spin correlation functions $\langle S_j^z(t)S_0^z(0) \rangle$,

$\langle S_j^+(t)S_0^-(0) \rangle$ and $\langle S_j^-(t)S_0^+(0) \rangle$, respectively [34]:

$$S^{z,\pm}(q, \omega) = \sum_j e^{-iqj} \int_{-\infty}^{\infty} dt e^{i\omega t} \langle S_j^{z,\pm}(t)S_0^{z,\mp}(0) \rangle_T,$$

$$T_1^{-1} \propto \frac{\gamma_n^2}{\gamma_e^2} \lim_{\omega \rightarrow 0} \sum_q |A_{\parallel}(q)|^2 S^z(q, \omega) + |A_{\perp}(q)|^2 [S^{\pm}(q, \omega) + S^{\mp}(q, \omega)]. \quad (1)$$

Here q is the wave vector, $\langle \dots \rangle_T$ means the thermal average, $\gamma_{e/n}$ are the gyromagnetic ratios of the electron and the probed nucleus, and $A_{\parallel,\perp}(\vec{q})$ are the hyperfine form factors of the probed nucleus. The subscripts \parallel and \perp denote the hyperfine tensor components generating the transversal components of the fluctuating local field at the nuclear site due to the longitudinal $\langle zz \rangle$ and transversal $\langle +- \rangle$ spin-spin correlations, respectively. For $\hbar\omega_{\text{NMR}} \ll k_{\text{B}}T$, $S^{z,\pm}(q, \omega) \propto \chi''_{z,\pm}(q, \omega)k_{\text{B}}T/\hbar\omega_{\text{NMR}}$, where $\chi''_{z,\pm}(q, \omega)$ is the imaginary part of the dynamical electron spin susceptibility, ω_{NMR} is the NMR frequency, k_{B} and \hbar are the Boltzmann's constant and the reduced Planck constant, respectively. Thus at small NMR frequencies, $1/T_1 \propto \sum_q \chi''(q, \omega \rightarrow 0)T$.

Generally, filtering effects may occur such that the hyperfine coupling is peaked (or zero) for certain q -vectors. However, the crystal structure of LiCuSbO_4 indicates that both Li sites are coupled to several Cu sites from different chains, suggesting a rather weak dependence of $A_{\parallel,\perp}$ on q . Since the coupling between the ${}^7\text{Li}$ nuclear spin and the Cu spins is of dipolar nature both the longitudinal and the transversal terms in Eq. (1) are expected to contribute to the relaxation. Indeed, our estimates with the dipolar hyperfine model have revealed comparable contributions from $\langle zz \rangle$ and $\langle +- \rangle$ correlations to the transversal field at both Li sites (see, Suppl.).

Field dependence of T_1^{-1} . In weakly coupled unfrustrated critical simple AFM Heisenberg chains in the paramagnetic state far above the Neél ordering temperature

$T_N \ll T \ll J/k_B$, the rate T_1^{-1} in general *continuously increases* with decreasing T and/or increasing the magnetic field H up to the saturation field and tends to diverge by approaching T_N . This is mainly due to the growth of the $\langle S_j^+(t)S_0^-(0) \rangle$ correlation function with increasing H and decreasing T whereas $\langle S_j^z(t)S_0^z(0) \rangle$ decays smoothly following a power law [35–37].

In LiCuSbO_4 , however, T_1^{-1} shows a non-monotonous and even contrasting behavior with respect to temperature and magnetic field. At relatively small fields the low-temperature region is determined by a more or less sharp increase of $T_1^{-1}(T)$ (Fig. 5) pointing to the vicinity of a critical magnetically ordered state at a lower tem-

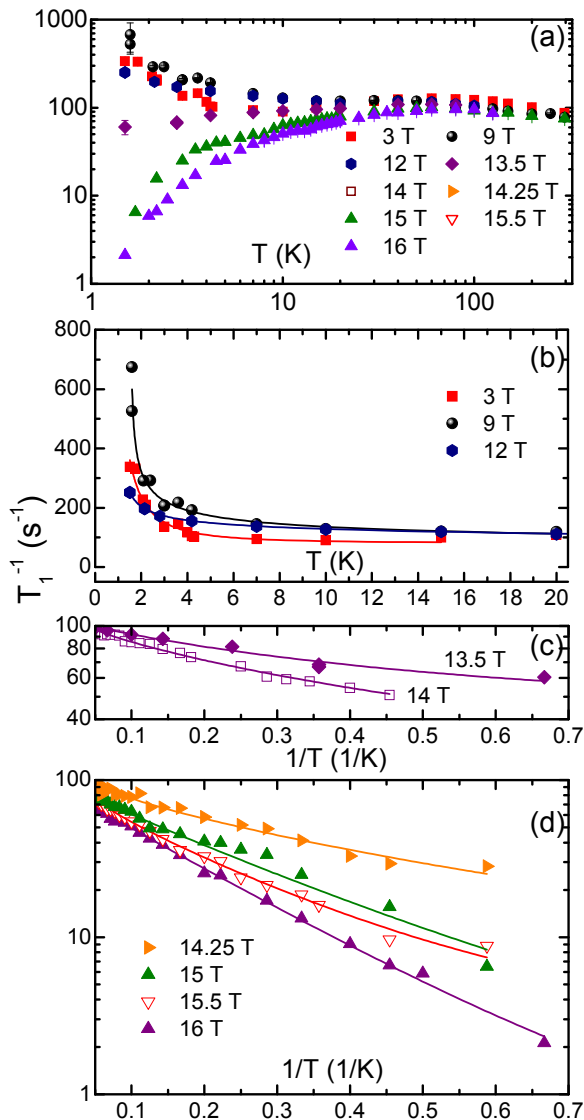


FIG. 5. (a) T_1^{-1} vs. temperature for different magnetic fields; (b) The $T_1^{-1}(T)$ dependence at $T < 20$ K for 3 T, 9 T and 12 T; (c,d) T_1^{-1} vs. inverse temperature T^{-1} at $T < 20$ K for fields > 13 T. Solid lines in (b), (c) and (d) are model curves according to Eq. (3).

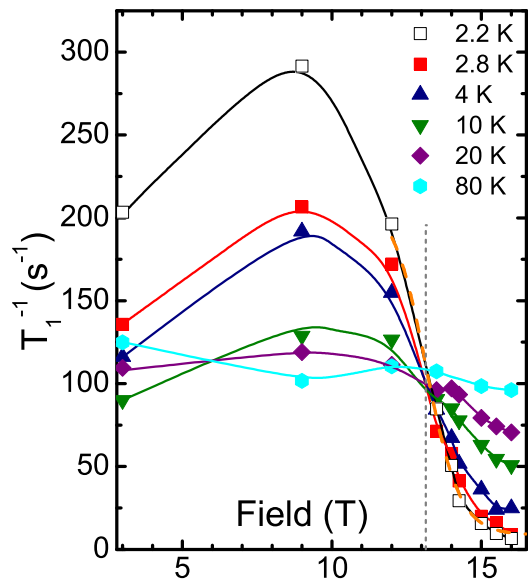


FIG. 6. The extracted spin-lattice relaxation rate $1/T_1$ vs. external magnetic field for selected temperatures. Full lines are guides for the eye. The isosbestic point (IBP) near ~ 13 T is indicated by the vertical dashed line. The dashed orange curve is the fit to Eq. (2). (see the text)

perature. Especially at $H = 9$ T the increase is substantially more pronounced than at lower fields such as for 3 T indicating an increase of the ordering temperature of the presumable magnetic phase. Such a behavior is not expected for an ordinary antiferromagnetic Néel state where T_N is usually suppressed by an external magnetic field. In fact, the field region around 9 T is also identified by the low-temperature anomaly in the magnetic specific heat in Ref. [26]. It has been conjectured in that work to be a signature of an unusual field-induced magnetic phase in LiCuSbO_4 .

One further and even more striking feature, which can be easily recognized in Fig. 5, is the occurrence of a threshold field of ~ 13 T that separates the upturn behavior from a drastic suppression of T_1^{-1} vs. T . Indeed, plotting these data points for fixed temperatures as a function of the field, yields a set of curves with a sharp general crossing point at $H_{c1} \approx 13$ T, usually denoted in the literature as an *isosbestic point* (IBP) [38] (Fig. 6). Since the nuclear T_1^{-1} is governed by fluctuating fields at the nuclear site produced by electron spins, the IBP at 13 T may be identified as the critical field that separates two regimes with *different* types of magnetic fluctuations to be discussed in detail below. Indeed, at low-temperatures $T \leq 10 - 15$ K which are of special interest here, the observed IBP coincides also with an inflection point (IFP). Using the generic linear field dependence $1/T_1 - \text{const} \propto (H - H_{c1})$ in the vicinity of an IFP at H_{c1} , it is tempting to generalize that linear behavior further into the nonlinear region at higher fields employing a quasi-exponential expression that captures also the field

region slightly smaller than H_{c1} :

$$T_1^{-1}(H) = \frac{1}{T_1(H_{c1})} \left[1 + 0.92 \tanh \frac{H - H_{c1}}{1.12A} \right]. \quad (2)$$

Here $1/T_1(H_{c1} = 13 \text{ T}) = 110 \text{ s}^{-1}$ and A is a dimensional constant taken as 1 T. As can be seen in Fig. 6, Eq.(2) describes the data in the considered field region for the lowest available temperature $T = 2.2 \text{ K}$ quite well. This way we arrive at a smooth transition across H_{c1} to a pronounced exponential-type behavior at high magnetic fields and low temperature.

Temperature dependence of T_1^{-1} . Importantly, as can be seen in a logarithmic plot of T_1^{-1} vs. T^{-1} in Figs. 5(c,d), a similar predominantly exponential behavior develops for the strongest fields also in the T -dependence of T_1^{-1} suggesting the opening of an energy gap for spin excitations. For a consistent analysis of the whole set of experimental $T_1^{-1}(T)$ curves we have used a phenomenological combined gapped and power-law ansatz:

$$T_1^{-1}(T) = C_1(H) \exp(-\Delta/T) + C_2(H)(T - T_c)^\beta. \quad (3)$$

Here, C_1 and C_2 are the weighting factors of the two contributions, Δ is the gap, and T_c and β are the critical temperature and the exponent of the power-law contribution, respectively. Possible T -dependences of the prefactors C_i remain unknown so far and have been not considered here. Then the $T_1^{-1}(T)$ dependences for all applied fields can be consistently modelled yielding a good description of the experimental data as shown in Fig. 5. The field dependences of the parameters of Eq. (3) are plotted in the Suppl., Fig. 13. The critical power-law behavior of $T_1^{-1}(T)$ at 3 T which sets in at $T \lesssim 7 \text{ K}$ is fully consistent with the growth of the short-ranged incommensurate correlations reported for this temperature regime in Ref. [26]. The fit requires a very small $T_c \sim 0.2 \text{ K}$ suggesting that the 3D long-range magnetic order, if present at all, is shifted to very low temperatures. At 9 T, however, T_c is pushed up to $\sim 1.5 \text{ K}$ indicating the proximity to a new, field-induced magnetic state that has been revealed in the specific heat data in Ref. [26]. Further increase of the field up to 12 T yields a reduction of T_c down to $\sim 1 \text{ K}$, again consistent with the fading of the magnetic anomaly in the specific heat [26]. Interestingly, the best agreement with experiment for $H = 12 \text{ T}$ requires a non-zero gap value $\Delta \sim 2 \text{ K}$ in the first term of Eq. (3) implying the contrasting gapped and critical power-law contributions to $T_1^{-1}(T)$ with $\Delta > 0$ and $\beta < 1$. By crossing the IBP $H_{c1} \approx 13 \text{ T}$ the critical growth of $T_1^{-1}(T)$ by lowering T turns into a decay corresponding to the sign change of the exponent β (Fig. 7, inset). Concomitantly the weight C_1 of the gapped term in Eq. (3) increases on expense of the decreasing weight C_2 of the power-law term. At the same time Δ increases non-linearly (Fig. 7).

Exclusion of an ordinary spin gap. In principle, there is a variety of conventional reasons for the opening of a gap

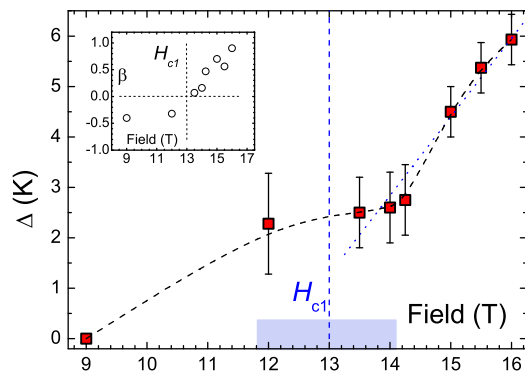


FIG. 7. Magnetic field dependence of the gap Δ (squares) evaluated using Eq. (3). Dashed line connecting the data points is guide for the eye. Dotted line is a linear fit revealing the slope $\Delta/H = 1.56 \text{ K/T}$; Inset: the same for the exponent β in Eq. (3) (circles). Vertical dashed lines denote the isobestic point $H_{c1} \approx 13 \text{ T}$. Shaded bar indicates a crossover region between the two distinct regimes of the ${}^7\text{Li}$ T_1 relaxation. (see the text)

in the spin excitation spectrum of a quantum magnet exposed to an external field. Generally, above saturation where the spins are fully polarized, all excitations acquire a gap that linearly scales with H . In the frustrated $J_1(\text{FM}) - J_2(\text{AFM})$ chain a two-magnon excitation is expected to have the lowest energy (see, e.g., [16]). In the case of LiCuSbO_4 , neglecting the non-linearity of the $\Delta(H)$ dependence in the crossover region, the increase of Δ amounts to $\Delta/H = 1.56 \text{ K/T}$ (Fig. 7). This slope is in accord with the Zeeman energy of the flip of a single spin, i.e. a one-magnon excitation, which with the g -factor $g = 2.18$ obtained in the ESR experiment would amount to $g\mu_B/k_B = 1.47 \text{ K/T}$. Correspondingly, the two-magnon slope should be $\sim 3 \text{ K/T}$. Anyhow, we note that it would be unreasonable to identify $H_{c1} \approx 13 \text{ T}$ as an effective saturation field. Our measurements of the static magnetization at very low T did not reveal a saturation of $M(H)$ even in 20 T [Fig. 3(a)]. This finding is supported by our DMRG results (see below) showing that in a situation of the symmetric exchange anisotropy present in LiCuSbO_4 , there is no well defined saturation field at all in a literal sense, i.e. the full saturation at $T = 0$ is achieved only asymptotically [Fig. 8(a)].

Another possible reason for a field induced gap could be the presence of staggered antisymmetric Dzyaloshinskii-Moriya (DM) interactions. Due to the low crystallographic symmetry, various DM interactions are generally allowed in LiCuSbO_4 (see below). Their magnitude in LiCuSbO_4 can be judged from the ESR data, because ESR is very sensitive to magnetic anisotropies. Assuming that the strongest antisymmetric DM coupling is present for the intra-chain NN bond with the DM vectors perpendicular to the Cu chain (see Fig. 1 and Suppl.), a strongly anisotropic gap should open for fields applied along the chain [39]. Such a gap results in a shift of the ESR signal for this field direction

proportional to H^3 at low temperatures $T < J/k_B$ [40, 41]. However, experimentally the frequency vs. magnetic field dependence of the ESR signal is linear within the error bars over a broad field range [Fig. 3(c)] which suggests that the staggered DM component of the antisymmetric exchange is small in LiCuSbO₄. The uniform component of the DM exchange can give rise to a field independent anisotropic gap which for certain field orientations may yield a splitting of the ESR signal [42, 43]. Such a fine structure of a powder ESR spectrum of LiCuSbO₄ is indeed found at high fields [Fig. 3(c)]. Its extend of the order $\approx \pm 30 \text{ GHz} = \pm 1.5 \text{ K}$ could give then the energy scale of the uniform DM component which is of a percent order of the isotropic and symmetric anisotropic exchange couplings as estimated from the magnetization data (see below).

Evidence for spin-nematicity. Ruling out the above discussed ordinary grounds for the field-dependent spin gap in LiCuSbO₄ enables us now to focus on a possible, more sophisticated reason for the gap opening by approaching the IBP $H_{c1} \approx 13 \text{ T}$ from the low-field side. According to the proposed theoretical precursor phase diagram of the isotropic frustrated $J_1 - J_2$ spin chain [11, 12, 14], sufficiently high magnetic fields yet smaller than the saturation field induce a multicomponent spin liquid including multi-magnon bound states. The two-magnon bound state ($p = 2$), corresponding to a precursor of a quadrupolar (spin-nematic) phase with a finite four-spin correlation function $\langle S_j^+ S_{j+1}^+ S_0^- S_1^- \rangle$ is the simplest one. In the presence of detrimental for the bound states interchain coupling a collinear and incommensurate quasi long-range ordered SDW₂-phase is more and more stabilized at the lower side of this field region since $\langle S_j^z S_0^z \rangle$ is the slowest decaying correlator. Above a certain crossover field the quadrupolar $\langle ++-- \rangle$ correlations might become nevertheless dominant yielding a competing quasi long-range ordered pronounced spin-nematic state at the higher field side [11, 12, 14]. In both SDW₂ and the spin-nematic parts of the quadrupolar TL liquid, $\langle S_j^+ S_0^- \rangle$ is expected to be gapped as demonstrated qualitatively for the special quasi-2D isotropic model case at $T = 0$ [17] which might probably hold in the case of relevant 3D interchain couplings at finite T , too. Finally, at very low fields magnon bound states as well as the collinear SDW fluctuations/order will be suppressed. Instead, a vector chiral order, which typically arises in a spin chain due to magnetic frustration somewhat modified quantitatively by possible DM couplings, turns out to be the ground state. In this phase the gap closes and the transverse $\langle S_j^+ S_0^- \rangle$ correlation becomes dominant.

Since quadrupolar correlations do not generate any fluctuating fields at a nuclear site, Sato *et al.* [36, 37] have proposed an indirect way to identify the quadrupolar phase of the isotropic $J_1(\text{FM}) - J_2(\text{AFM})$ chain and to distinguish between its SDW₂ and the spin-nematic dominated regions. It is predicted that T_1^{-1} due to longitudinal $\langle zz \rangle$ correlations should follow the power law

$\sim T^{2\kappa-1}$, where κ is the TL parameter. In the SDW₂ precursor phase $\kappa < 1/2$ and T_1^{-1} diverges with decreasing temperature whereas in the spin-nematic state $\kappa > 1/2$ and T_1^{-1} decays as $T \rightarrow 0$. In both regimes transverse $\langle +- \rangle$ correlations yield a gapped contribution to $T_1^{-1} \sim \exp(-\Delta/T)$.

It is reasonable to attribute incommensurate spin correlations observed in LiCuSbO₄ as well as a weak magnetic anomaly in the specific heat at low fields [26] with the onset of a conventional short-range ordered vector chiral phase. The proximity to this phase is reflected in an increase of the ⁷Li relaxation rate at low T due to the growth of $\langle +- \rangle$ correlations. From the fit with Eq. (3) a long-range vector chiral order due to interchain coupling could be realized only at very low temperatures $T_c \sim 0.2 \text{ K}$ and in fact was not observed down to 0.1 K [26]. A new field-induced magnetic phase at higher fields and higher temperatures yielding a strong anomaly in the magnetic specific heat [26] can thus be naturally ascribed to the short-range ordered SDW₂ phase. In this regime the observed strong enhancement of $T_1^{-1}(T)$ should be due to the dominant longitudinal $\langle zz \rangle$ correlations which according to the modelling of the 9 T data with Eq. (3) should yield a long-range SDW₂ order below $T_c \sim 1.5 \text{ K}$ [44].

Further increasing the field up to 12 T yields a weakening of the $\langle zz \rangle$ power law contribution on which background a gapped $\langle +- \rangle$ contribution to the $T_1^{-1}(T)$ dependence with $\Delta \sim 2 \text{ K}$ becomes distinguishable. This clearly suggests the destabilization of the SDW₂ state which is also reflected in the decreased value of $T_c \sim 1 \text{ K}$ in the model dependence (Suppl., Fig. 13).

The vanishing of the power-law contribution at the critical IBP $H_{c1} \approx 13 \text{ T}$ signals then a crossover to the distinctive spin-nematic state with dominant quadrupolar $\langle ++-- \rangle$ correlations. In this regime the $\langle zz \rangle$ correlations are decaying with lowering T which corresponds to the sign change of the power-law exponent κ [36, 37]. This is indeed the case for LiCuSbO₄ (Fig. 7, inset). The now decaying power law contribution to T_1^{-1} loses progressively its weight with increasing field whereas the gapped contribution becomes dominant (Suppl., Fig. 13). Indeed, as it has been emphasized in Ref. [17] the gapped excitation spectrum is a distinct feature of the spin-nematic state of the weakly coupled 1D-chains with only a weak soft mode in the longitudinal $\langle zz \rangle$ channel [17, 45]. Thus, regardless of the specific details the above analysis points at a rather broad stability range of the spin-nematic state in LiCuSbO₄ above the narrow crossover region at the IBP field $H_{c1} \approx 13 \text{ T}$.

Owing to small and/or frustrated interchain couplings in LiCuSbO₄, long-range order of any kind is likely to be suppressed by quantum fluctuations to very low T . Therefore, the distinct state around H_{c1} identified in the NMR experiments in the accessible temperature range should be considered as the TL quadrupolar *liquid* with dominant SDW₂ correlations for $H \lesssim H_{c1}$ and with dominant spin-nematic correlations for $H \gtrsim H_{c1}$. In a recent

2D-model the SDW₂ state is shown to dominate over a broad magnetic field range squeezing a nematicity region very near to the saturation field [17]. In contrast, the SDW₂ liquid phase in LiCuSbO₄ appears to be confined to a restricted field range below $H_{c1}(H)$ at lower T not covered by the present NMR study, giving much place to the competing pronounced spin nematic state in an extended field range above H_{c1} . This may be related to the specific interchain couplings in LiCuSbO₄ and the detrimental influence of DM couplings favoring noncollinear order and thus destabilizing any collinear SDW _{p} , ($p \geq 2$) state. In fact, a weak interchain coupling is favorable for a pronounced multipolar state [24] but detrimental for any dipolar SDW-state or spiral state since the Néel temperature scales usually with coherent interchain coupling which suppress the detrimental thermal fluctuations. Thus possible structural disorder, the presence of DM interactions and strongly frustrating interchain couplings allowed by the low-symmetry (Fig. 1) are also not favorable for any magnetic dipolar ordering. The mentioned NN symmetric exchange anisotropy stabilizes the nematicity as will be shown below (see also Ref. [24]). All these circumstances are obviously favorable for a stabilization of a nematic state in a broad region above H_{c1} as depicted in the schematic phase diagram of LiCuSbO₄ in Fig. 9. Certainly, there must be also a second "upper" critical field H_{c2} framing the stability region of the strong nematic state in LiCuSbO₄. This calls for further experimental studies of LiCuSbO₄ at higher fields and also at lower temperatures beyond the scope of the present work.

Theory. *Band structure calculations.* As in other related materials (see., e.g., Refs. [20–22, 28]), the edge-sharing geometry of the CuO₄ plaquettes in the CuO₂ chains in LiCuSbO₄ (Fig. 1) is expected to give rise to the usual frustrated magnetism due to the presence of oxygen mediated frustrated AFM NNN intra-chain couplings. The nearly 90° Cu-O-Cu bond angle, i.e. 93°, points to FM NN intra-chain interactions due to the presence of a sizable direct FM coupling $K_{pd} \sim 100$ meV between two holes residing on neighboring sites with Cu $3d$ and O $2p$ orbitals and a significant compensation of the AFM NN superexchange contributions.

We have performed DFT and DFT+ U bandstructure calculations with the aim to understand (i) the amount of interchain couplings and (ii) the magnitude of the intra-chain couplings. With respect to (i) we have analyzed the dispersion of bands and found pronounced 1D van Hove singularities near the Fermi level. Thus, we have confirmed the nearly 1D behavior of LiCuSbO₄. Then, in general, the exchange coupling strength can be estimated simply by the AFM contribution $J_1 = 4t_1^2/U_{\text{eff}}$, where $U_{\text{eff}} \sim \Delta_{pd} \approx 3$ to 4 eV is the effective Coulomb repulsion within a *single*-band type approach for the Cu-sites with NN transfer integral t_1 . The frustrating J_2 is measured by the analogous expression using the NNN transfer integral t_2 instead ignoring a much weaker direct FM contribution as compared to

that of the NN bond ($K_{pd} \gg K_{pp}$) and the small hole occupation at O $2p$ orbitals. Note that applying such a simple model to charge transfer insulators as cuprates, one is left with an effective onsite repulsion U of the order of the Cu $3d$ -O $2p$ onsite energy difference which is significantly smaller than the $U_d \sim 5.5$ eV at Cu sites employed in the DFT+ U calculations or in more sophisticated five-band pd Hubbard models [46, 47] to be considered for to the case of LiCuSbO₄ elsewhere. To check this simple first approach, we have determined the Cu-Wannier functions which contain also the essential O $2p$ contributions. Their tails point to the important coupling directions. In fact, a closer inspection of the crystal structure reveals nonequivalent "left" and "right" NN intra-chain bonds (Fig. 1). This gives rise to alternating NN transfer integrals ($t_1 \neq t'_1$). The one-band fit results in the following transfer integrals (given in meV): $t_1 = -95.51$, $t'_1 = 56.44$, $t_2 = 56.96$, and $t_3 = -11.88$, $t'_3 = -16.57$. Then the mean NN transfer integral \bar{t}_1 would provide an AFM superexchange contribution to J_1^e for an equidistant chain of about 67 K which for a typical J_1^e of about -80 K like in linarite (see, Refs. [22, 48] and references therein) corresponds to an FM contribution of -147 K. As a result we arrive at a sizable splitting of the two NN exchange integrals: $J_1 \approx -160$ K and $J'_1 \approx -90$ K, whereas $J_2 \approx 37.6$ K, only. Thus, within a 1D picture we are left with a dominant FM total NN coupling and an unrenormalized mean frustration parameter $\bar{\alpha} = J_2/[(J_1 + J'_1)/2] \sim 0.3$. This value is close to that ($\alpha = 0.28$) estimated from the fitting of the observed magnetization curve by the DMRG calculations (see below).

Symmetry analysis and the role of DM interactions.

The crystal structure of LiCuSbO₄ is described by the polar space-group Cmc2₁ [26]. The low symmetry implies modifications of the standard J_1 - J_2 spin-model to describe the chains of the edge-shared CuO₄ square-like plaquettes running in a -direction. More details of our symmetry analysis are given in the Supplement. In particular, because of the low symmetry, antisymmetric Dzyaloshinskii-Moriya (DM) interactions are allowed for the NN bonds along the spin-chains, $E_D = \mathbf{D}_\nu \cdot (\mathbf{S}_i \times \mathbf{S}_{i+\nu})$ and have *both* a homogeneous and a staggered component. These microscopic antisymmetric exchange interactions are caused by the relativistic spin-orbit interactions and compete with the isotropic exchange interactions.

To fit the experimental data for LiCuSbO₄, Dutton *et al.* [26] assumed in their model the presence of this exchange anisotropy for the NN bond, while neglected the anisotropic terms *linear* in $|\mathbf{D}_\nu|$. However, this could yield an unrealistic picture for the basic magnetic couplings in LiCuSbO₄. The determined strength of the effective anisotropic coupling constant is large and would imply an unusual order of magnitude $|\mathbf{D}_1|/|J_1| \sim 1$. The presence of the relativistic antisymmetric exchange

in crystals belonging to the crystal classes $2mm$ or C_{2v} may give rise to two rather different states [49]: weak ferromagnetism or more generally canting of spins with a net magnetization can be derived by the staggered DM couplings. Besides, the acentric crystal structure also allows for the presence of ‘*inhomogeneous DM couplings*’, [49] that derive from the homogeneous part of the DM interaction. It is known that this type of couplings can suppress any long-range ordered states and may be related to the absence of magnetic ordering down to ~ 0.1 K in LiCuSbO_4 .

DMRG-calculations. The main aim of this part is to present an analysis of a novel anisotropy mechanism based on the low-symmetric NN exchange anisotropy, which in addition to the J_1 - J_2 frustration, stabilizes a nematic phase in a moderate high-field region to be specified below. We present a first brief analysis also of the effect of weak homogeneous and staggered NN DM couplings which were found not to destroy the nematicity although some weakening has been observed.

Fig. 8(a) shows the magnetization curve $M(H)$ measured at $T = 0.45$ K. Noteworthy, a full saturation is not reached even in the highest accessible field of 20 T. Although this is reminiscent of a typical feature of $M(H)$ at high temperature, the observation temperature is now low enough to prevent a significant finite-temperature effect. To provide a reasonable explanation for this feature, we introduce a 1D frustrated Heisenberg model with an xyz exchange anisotropy and a magnetic field H along the z axis. The Hamiltonian is then given by

$$\mathcal{H} = \sum_{i,\gamma=x,y,z} J_1^\gamma S_i^\gamma S_{i+1}^\gamma + J_2 \sum_i \mathbf{S}_i \cdot \mathbf{S}_{i+2} + H \sum_i S_i^z, \quad (4)$$

where J_1^γ and J_2 are the NN FM and the NNN AFM exchange couplings, respectively, and S_i^γ is the γ -component of the spin-operator \mathbf{S}_i . When $H \gg J_1^\gamma, J_2$, by taking the fully polarized FM state as non-perturbative state, its energy is lowered by $\Delta E = (J_1^x - J_1^y)^2 / [32(H - J_1^x - J_2)]$ through the second-order process of an individual double spin-flip. Therefore, the magnetization behaves like $M_S - M \propto (J_1^x - J_1^y)^2 / H$ at high fields and saturates its maximum value M_S only at $H = \infty$, only. We have calculated the magnetization curve using the DMRG technique. By fitting the experimental curve, we have found a possible parameter set: $J_1^z = -546$ K, $(J_1^x / J_1^z, J_1^y / J_1^z) = (1.07, 0.99)$, and $J_2 = 153$ K. Note that these numbers are effective values in the 1D limit, which can be significantly different from the bare values of NN and NNN exchange couplings determined by the DFT+ U calculations. Other contributions such as the interchain and longer-range exchange couplings are renormalized into them. As a related similar example we refer the reader to linarite [22, 48].

More interestingly, an exotic nematic state is established by the xyz exchange anisotropy [50]. The xy com-

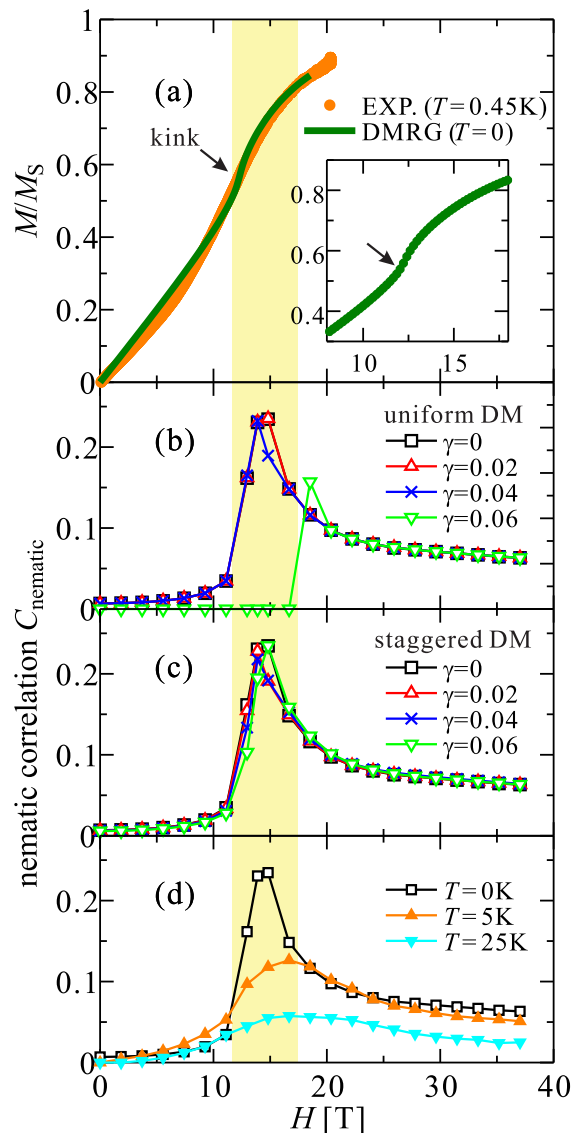


FIG. 8. (a) Experimental magnetization curve at 0.45 K and theoretical magnetization curve calculated for $(J_1^x, J_1^y, J_1^z) = (-1.07, -0.99, -1)$ and $J_2 = 0.28$. Inset: enlarged figure around kink in the theoretical curve. (b) Nematic correlation for a homogeneous DM coupling $\gamma = 0, 0.02, 0.04$, and 0.06 . (c) the same for a staggered DM coupling. (d) Temperature dependence of the nematic correlation. The shaded area depicts the field range where a spin gap was observed in the NMR experiment.

ponents of the first term of Eq. (4) can be divided into an exchange term $\frac{J_1^x + J_1^y}{4}(S_i^+ S_{i+1}^- + h.c.)$ and a double spin-flip term $\frac{J_1^x - J_1^y}{4}(S_i^+ S_{i+1}^+ + h.c.)$. The latter seems to create an attractive interaction among the parallel spins. Therefore, a 2-magnon bound state, i.e., a nematic state, may be naively expected at high field \mathbf{s} in the presence of xyz exchange anisotropy. To check this possibility, we have calculated the nematic correlation function as an

indicator of magnon pairing

$$\begin{aligned} C_{\text{nematic}} &= \langle S_i^- S_{i+1}^- \rangle - \langle S_i^- S_{i+\infty}^- \rangle \\ &\equiv \langle S_i^+ S_{i+1}^+ \rangle - \langle S_i^+ S_{i+\infty}^+ \rangle. \end{aligned} \quad (5)$$

Note that this correlation vanishes for lacking xyz exchange anisotropy, because there is no overlap between different S^z sectors. The nematic correlation for our parameter set is plotted as a function of H in Fig. 8(b). It is significantly enhanced just above the kink position of the theoretical magnetization curve. This field range with the enhanced correlation agrees well with that region where the spin gap has been experimentally observed, namely, in between $H = 13 - 16$ T. A similar nematicity scenario has been proposed in our recent work devoted to linarite [22], but there yet not fully confirmed experimentally due to a phase separation and other experimental and physical difficulties. Furthermore, we have also studied the effect of additional uniform or staggered DM couplings allowed by the crystallographic symmetry as mentioned above $\mathcal{H}_{\text{DM}} = \sum_i \mathbf{D} \cdot (\mathbf{S}_i \times \mathbf{S}_{i+1})$ with $\mathbf{D} = (0, 0, \gamma)$. As a result we found that the nematic state is *hardly* affected by a weak DM coupling for $\gamma < 0.05$. The effect of a staggered DM interaction is even weaker than that of a uniform one. For simplicity, the dimerization of the NN exchange couplings, suggested by the DFT, was not taken into account in the present DMRG calculations. However, the stability of the nematic state is mostly related to the magnitude of the exchange anisotropy and is less affected by the dimerization. Also, the T -dependence of the correlation is plotted in Fig. 8(d). We can see that the sharp enhancement of the correlation around $H = 13$ T at $T = 0$ disappears for higher T which points to existence of the mentioned above upper critical field.

Thus, we are confronted with a somewhat unusual situation: the pronounced spin gap and the strongly enhanced nematic correlations are, in a literal sense, not the result of the occurrence of a novel order parameter associated with symmetry breaking due to a second order phase transition from a high temperature and low-field para-phase, since at low fields the nematic order at $T = 0$ already exists albeit at a low level. Instead, based on our calculations and in accord with the experimental data, we suggest a crossover transition from a weak nematic state in a narrow field range at about 13 T to a pronounced nematic state up to at least 16 T to 20 T to be followed by a broad field range where it decreases again (Figs. 8 and 9).

Such transitions without a symmetry change of the macroscopic order parameter are reminiscent of mesoscopic liquid-liquid transitions in ordinary liquids such as, for instance, in phosphorus and water governed by the *quantitative* change of a correlation function, only [51–53]. With increasing T these changes are smeared out and the consequences of the suppressed nematic order parameter are difficult to be observed. In such a complex situation further experimental and theoretical

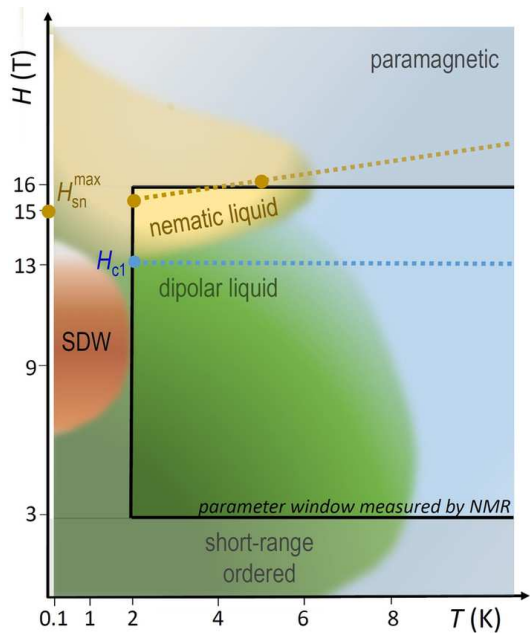


FIG. 9. Schematic phase diagram of LiCuSbO₄. Blue, dark green, and dark red regions reproduce approximately the diagram of Dutton *et al.* based on the analysis of the specific heat and magnetization data (Fig. 3 in Ref. [26]). The dark red area is suggested to present an anomalous SDW phase, whereas the dark yellow area depicts an envisaged stability region of the proposed nematic state. The region measured by the NMR in the present work is marked by the black rectangle. The blue dashed line denotes the isosbestic field H_{c1} (cf. Fig. 6). The brown closed circles labelled $H_{\text{sn}}^{\text{max}}$ connected with the dashed line depict the field of the maximum of the spin-nematic correlation function as found in the DMRG analysis (cf. Fig. 8).

studies beyond the scope of the present work are necessary to refine the parameters of our proposed model and to take into account explicitly the weaker couplings and modifications suggested by the real structure including also impurities or defects.

Summary

In conclusion, we have presented experimental and theoretical evidence for the occurrence of a distinctive spin-nematic state in the frustrated anisotropic spin chain cuprate LiCuSbO₄. This state emerges above an isosbestic point $H_{c1} \approx 13$ T detected in the field dependence of the ⁷Li NMR relaxation rate T_1^{-1} at low temperatures. The analysis of the temperature dependences of T_1^{-1} reveals that H_{c1} separates a lower-field regime with strong enhancement of T_1^{-1} at low T from a higher-field regime with a sharp decrease of $T_1^{-1}(T)$. The former is ascribed to diverging longitudinal spin correlations typical for a multipolar SDW liquid whereas the latter is due to the power-law like decaying longitudinal and gapped transverse spin correlations characteristic of the spin-nematic liquid. Theoretical analysis justifies the occurrence of this "hidden" spin-nematic state in

LiCuSbO₄ in an extended field range above H_{c1} . A broad range of stability of this spin-nematic state unexpected in the corresponding isotropic spin-chain model can be ascribed to the presence of exchange anisotropies. Indeed, as is found in the DMRG calculations it can be due to a special low-symmetry symmetric exchange anisotropy which is reflected in the high-field magnetization data. The missing SDW-type magnetic ordering at lower fields might be ascribed to some structural disorder and/or frustrated interchain interactions caused by DM couplings allowed in this low-symmetry crystal structure in general. The small but finite DM coupling favoring a noncollinear spin arrangement could be responsible for the suppression of the otherwise strongly competing anomalous collinear SDW₂ phase. On the other hand, according to complete diagonalization and DMRG studies in high magnetic fields the presence of a weak DM interaction, uniform or staggered, identified in the symmetry analysis of LiCuSbO₄ and assessed with ESR, are not detrimental for nematicity. Merely an alteration of the two NN exchange couplings may somewhat reduce the binding energy of two-magnon bound states as compared to equal NN bonds. The remarkable interplay of symmetric and antisymmetric exchange anisotropies with sizable frustration is of general interest in modern quantum magnetism and calls for deeper theoretical and experimental studies.

Methods

Sample synthesis and characterization. Green polycrystalline sample of LiCuSbO₄ was prepared through solid-state reaction using stoichiometric mixture of dried Li₂CO₃ (99.98 %, Chempur), CuO (99.95 %, Aldrich) and Sb₂O₅ (99.9 %, Alfa Aesar). The mixture of the precursor compounds was homogenized by grinding in a mortar and pestle, followed by a 16 h sintering at 700 °C. The sample was subsequently grounded, pressed into pellets and fired at 1000 °C for 48 h. Pure LiCuSbO₄ phase was obtained after annealing of the pellets at 1050 °C for 24 h under dried oxygen flow. Phase purity of the products was assessed by powder X-ray diffraction, by using a STOE Stadi P powder diffractometer with Mo K_{α1} radiation. The diffractometer is equipped with a curved Ge (111) monochromator and a 6° linear position sensitive detector (DECTRIS MYTHEN 1 K detector). Powder x-ray diffraction data were analyzed with the Rietveld method using the FULLPROF in the WinPlotR program package program [54]. The background was fitted using linear interpolation between selected points. The March-Dollase model for preferred orientation was used in all of the refinements, and a pseudo-Voigt function was used as the peak-shape model. As refinable parameters background, scale factor, half width, Caglioti variables (U, V, W), lattice parameters, asymmetries and the overall temperature factor were allowed. Based on Rietveld analysis of the powder x-ray diffraction data (Fig. 10), the main phase is LiCuSbO₄ 96.93(6) wt % (or-

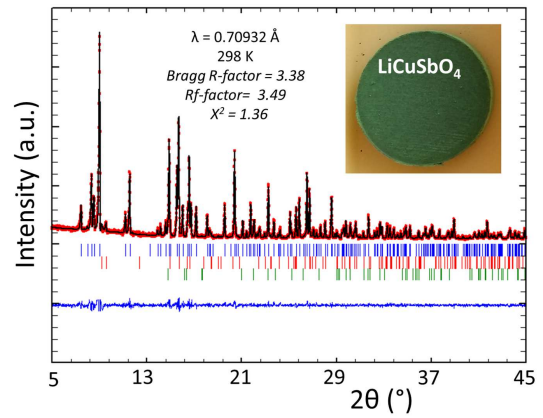


FIG. 10. Calculated and observed X-ray diffraction pattern of the Rietveld refinement for LiCuSbO₄. The difference curve is shown in blue; reflection positions are indicated by the vertical lines for LiCuSbO₄ (blue), LiSbO₃ [2.36(5) wt %] (red) and CuO [0.72(1) wt %] (green) impurity phases. ($\lambda = 0.70932 \text{ \AA}$, Bragg R-factor: 3.38 %; Rf-factor = 3.49 %; Bragg R-factor = $\sum |I_{ko} - I_{kc}| / \sum I_{ko}$; Rf-factor = $[(N - P) / \sum w_i y_{io}^2]^{1/2}$). The inset shows optical image of a typical green pellet of polycrystalline sample of LiCuSbO₄ after annealing in dried oxygen flow.

thorhombic, Cmc21, $a = 5.7493(1) \text{ \AA}$, $b = 10.8828(2) \text{ \AA}$, $c = 9.7429(1) \text{ \AA}$). LiSbO₃ 2.36(5) wt % (orthorhombic, Pnma, $a = 5.1756(4) \text{ \AA}$, $b = 4.9092(3) \text{ \AA}$, $c = 8.4887(6) \text{ \AA}$) and 0.72(1) wt % CuO are two minor impurity phases. The amount of foreign phase is very similar to the previous report in Ref. [26].

Nuclear magnetic resonance. NMR spectra were obtained with a Tecmag Apollo spectrometer and a standard sample probe from NMR Service GmbH. The magnetic field has been applied by a 16 T Oxford Instruments superconducting magnet. Temperatures were regulated by a ⁴He variable temperature insert (VTI). Temperatures below 4.2 K were achieved by pumping on the VTI. At high temperatures and small fields, Fourier transformations (FFT) of the spin echo covered the whole spectral width. At lower temperatures, we swept the frequency and summed up the FFT's to obtain the complete spectrum. The spectra at 15 T below 10 K have been obtained by field sweeps, and converting into frequency sweeps. This is easily possible due to the negligible quadrupole interaction. We have confirmed the correctness of this procedure at higher temperatures. The spin lattice relaxation rate, T_1^{-1} , has been measured by standard saturation recovery at the peak of the spectra. The nuclear magnetization, M_0 , has been saturated by a train of radio frequency pulses, before measuring the recovered nuclear magnetization, $M(\tau)$, depending on the time τ between the saturation train and the spin echo sequence.

Electron spin resonance. ESR spectra were measured with the Terahertz ESR Apparatus (TESRA-IMR) installed in the magnetism division of Institute of Materials Research, Tohoku University [55]. As sources

of the microwave radiation up to 450 GHz conventional Gunn oscillators were employed. The signals were detected with an InSb detector. Pulse magnetic fields up to 20 T were generated with a solenoid magnet and a 90 kJ capacitor bank. The sample temperature was regulated with a ^3He cryostat. Additional ESR measurements were performed at the IFW Dresden with a home-made multi-frequency high-field ESR spectrometer at magnetic fields up to 16 T and at frequencies ν up to 400 GHz [56]. For the generation and detection of the microwave radiation millimeter wave backward oscillators and an InSb bolometer from QMC Instruments Ltd., as well as a millimeter wave network analyzer from AB Millimetre, have been used. DC magnetic fields were obtained with a solenoid superconducting magnet from Oxford Instruments equipped with a ^4He variable temperature insert.

Static magnetization. Temperature dependence of the static magnetic susceptibility in fields up to 5 T in the temperature range $T = 2 - 300$ K was measured with the SQUID magnetometer from Quantum Design. Static magnetization in fields up to 20 T was measured with a standard inductive method using compensated pickup coils and a nondestructive pulse magnet (for details see Ref. [57]). The sample was immersed into liquid ^3He to reach a temperature as low as 0.45 K.

Density functional calculations. Relativistic density functional (DFT) electronic structure calculations were performed using the full-potential local orbital FPLO code [58–60], version fplo14.00-49. For the exchange-correlation potential, within the local density (LDA) and the the general gradient approximation (GGA) the parametrizations of Perdew-Wang [61] and Perdew-Burke-Ernzerhof [62] were chosen, respectively. Both exchange-correlation potential yielded essentially the same band structure. To obtain precise band structure information, the final calculations were carried out on a well converged mesh of 4800 k -points (20x20x12 mesh, 1332 points in the irreducible wedge of the Brillouin zone). For our calculations, we used the experimental crystal structure of Ref. [26]. However, to model the Li split positions Li1a (4a), Li1b (4a) and Li2 (8b), we used averaged coordinates: Li1 (4a) 0.0 0.3610 0.6974 or the coordinates of the nearby high symmetry position Li2 (4a) 0. 0.0002 0.2660; Li split positions have been successfully modeled this way for the related edge-sharing chain compound LiZrCuO_4 [63].

Acknowledgments

The authors thank C. Blum and L. Giebeler for assistance with the XRD measurements, and A. Wolter-Giraud, F. Hammerath, Y. Utz and A. Smirnov for useful discussions. This work has been supported in part by the Deutsche Forschungsgemeinschaft through grants SFB 1143 (S.N.), KA 1694/8-1 (V.K.), GR 3330/4-1 (H.-J.G.), through the Emmy Noether Programme in the projects WU595/3-1, and WU595/3-2 (S.W.). The work of E.V. and M.I. has been supported in part by project RFBR 14-02-01194. V.K. gratefully acknowledges financial support during his stay in Sendai from the International Collaboration Centre, Institute of Materials Research, Tohoku University, Sendai. S.-L.D and S.N. thank R.O. Kuzian, J. van den Brink, C. Agrapidis, A. Tsirlin, A. Zvyagin, P. Mendels, H. Kühne, S. Zvyagin, M. Zhitomirsky, and O. Starykh for discussions and stimulating interest.

Author contributions

H.-J.G., M.I and E.V. conducted the NMR studies. H.N., V.K., and A.A. conducted the ESR studies. H.N. performed the high-field magnetization measurements. M.I.S. and S.W. synthesized and characterized the samples. S.N. performed the DMRG-calculations and invented the nematicity scenario based on the special anisotropic NN exchange. J.R. carried out the complete diagonalizations to study effects of the DM interactions. H.R. performed the LDA-FPLO electronic structure calculations for LiCuSbO_4 , invented its $(J_1, J'_1) - J_2$ model, and estimated the leading exchange couplings. U.R., H.R. and S.-L.D. made the symmetry and phenomenological analysis including the isosbestic point. L.S. calculated the hyperfine tensor. V.K., E.V., S.-L.D. and B.B. designed the project. All coauthors participated actively in the discussion and selection of the various experimental and theoretical results presented in this paper and worked out the final concept of the paper. V.K. and S.-L.D. wrote the paper with important contributions to all its parts from all other coauthors.

Additional information

Competing financial interests: The authors declare no competing financial interests.

-
- [1] E. Fradkin, S. A. Kivelson, M. J. Lawler, J. P. Eisenstein, and A. P. Mackenzie, “Nematic Fermi fluids in condensed matter physics,” *Annu. Rev. Condens. Matter Phys.* **1**, 153 (2010).
 [2] S. Sachdev, “Quantum magnetism and criticality,” *Nature Physics* **4**, 173 (2008).
 [3] L. Balents, “Spin liquids in frustrated magnets,” *Nature*

- 464**, 199 (2010).
 [4] K. Penc and A. M. Läuchli, “Spin nematic phases in quantum spin systems,” in *Introduction to Frustrated Magnetism*, Springer Series in Solid-State Sciences, Vol. 164, edited by C. Lacroix, P. Mendels, and F. Mila (Springer-Verlag, Berlin, Heidelberg, 2011) p. 331.
 [5] H.-J. Mikeska and A. Kolezhuk, “One-dimensional mag-

- netism,” in *Quantum Magnetism*, Lect. Notes Phys., Vol. 645, edited by U. Schollwöck, J. Richter, D. J. Farnell, and R. Bishop (Springer-Verlag, Berlin, Heidelberg, 2004) p. 1.
- [6] C. K. Majumdar and D. K. Ghosh, “On next-nearest-neighbor interaction in linear chain. I,” *J. Math. Phys.* **10**, 1388 (1969).
- [7] F. Haldane, “Spontaneous dimerization in the $S = 1/2$ Heisenberg antiferromagnetic chain with competing interactions,” *Phys. Rev. B* **25**, 4925(R) (1982), erratum - *Phys. Rev. B* **26**, 5257 (1982).
- [8] A. Chubukov, “Chiral, nematic, and dimer states in quantum spin chains,” *Phys. Rev. B* **44**, 4693 (1991).
- [9] L. Kecke, T. Momoi, and A. Furusaki, “Multi-magnon bound states in the frustrated ferromagnetic one-dimensional chain,” *Phys. Rev. B* **76**, 060407 (2007).
- [10] R. Kuzian and S.-L. Drechsler, “Exact one- and two-particle excitation spectra of acute-angle helimagnets above their saturation magnetic field,” *Phys. Rev. B* **75**, 024401 (2007).
- [11] T. Vekua, A. Honecker, H.-J. Mikeska, and F. Heidrich-Meisner, “Correlation functions and excitation spectrum of the frustrated ferromagnetic spin- $\frac{1}{2}$ chain in an external magnetic field,” *Phys. Rev. B* **76**, 174420 (2007).
- [12] T. Hikihara, L. Kecke, T. Momoi, and A. Furusaki, “Vector chiral and multipolar orders in the spin- $\frac{1}{2}$ frustrated ferromagnetic chain in magnetic field,” *Phys. Rev. B* **78**, 144404 (2008).
- [13] A. Läuchli, J. Sudan, and A. Lüscher, “The frustrated ferromagnetic $S = 1/2$ Heisenberg chain in a magnetic field how multipolar spin correlations emerge from magnetically ordered states,” *J. Phys. Conf. Ser.* **145**, 012057 (2009).
- [14] J. Sudan, A. Lüscher, and A. Läuchli, “Emergent multipolar spin correlations in a fluctuating spiral: The frustrated ferromagnetic spin-1/2 Heisenberg chain in a magnetic field,” *Phys. Rev. B* **80**, 140402(R) (2009).
- [15] H. Ueda and K. Totsuku, “Magnon Bose-Einstein condensation and various phases of three-dimensional quantum helimagnets under high magnetic field,” *Phys. Rev. B* **80**, 14417 (2009).
- [16] M. Zhitomirsky and H. Tsunetsugu, “Magnon pairing in quantum spin nematic,” *EPL* **92**, 37001 (2010).
- [17] O. Starykh and L. Balents, “Excitations and quasi-one-dimensionality in field-induced nematic and spin density wave states,” *Phys. Rev. B* **89**, 104407 (2014).
- [18] A. Smerald and N. Shannon, “Theory of NMR $1/T_1$ relaxation in a quantum spin nematic in an applied field,” *Phys. Rev. B* **93**, 184419 (2016).
- [19] K. Nawa, M. Takigawa, M. Yoshida, and K. Yoshimura, “Anisotropic spin fluctuations in the quasi one-dimensional frustrated magnet LiCuVO_4 ,” *Journal of the Physical Society of Japan* **82**, 094709 (2013).
- [20] N. Büttgen, K. Nawa, T. Fujita, M. Hagiwara, P. Kuhns, A. Prokofiev, A. Reyes, L. Svistov, K. Yoshimura, and M. Takigawa, “Search for a spin-nematic phase in the quasi-one-dimensional frustrated magnet LiCuVO_4 ,” *Phys. Rev. B* **90**, 134401 (2014).
- [21] L. Prozorova, S. Sosin, L. Svistov, N. Büttgen, J. Kemper, A. Reyes, S. Riggs, A. Prokofiev, and O. Petrenko, “Magnetic field driven 2d-3d crossover in the $s = 1/2$ frustrated chain magnet LiCuVO_4 ,” *Phys. Rev. B* **91**, 174410 (2015).
- [22] B. Willenberg, M. Schäpers, J.-U. Hoffmann, A. Wolter, S.-L. Drechsler, M. Reehuis, B. Büchner, A. Studer, K. Rule, B. Ouladdiaf, S. Söllow, and S. Nishimoto, “Complex field-induced states in linarite $\text{PbCuSO}_4(\text{OH})_2$ with a variety of high-order exotic spin-density wave states,” *Phys. Rev. Lett.* **116**, 047202 (2016).
- [23] For completeness we note, that a suggested “bond-nematic” phase with a coexisting collinear SDW₂-magnetic structure and nematic fluctuations proposed in Ref. [64] has been arguably questioned in Ref. [17] based on the analysis of an isotropic quasi-2D field-theory model for interacting chains. The very broad phase below $H_{\text{sat}} \sim 43$ T was ascribed instead to the mentioned above SDW₂-phase, only.
- [24] S. Nishimoto, S.-L. Drechsler, R. Kuzian, J. Richter, and J. van den Brink, “Interplay of interchain interactions and exchange anisotropy: Stability and fragility of multipolar states in spin-1/2 quasi-one-dimensional frustrated helimagnets,” *Phys. Rev. B* **92**, 214415 (2015).
- [25] H. Onishi, “Effects of magnetic anisotropy on spin dynamics of ferromagnetic frustrated chain,” *J. Phys. Conf. Ser.* **592**, 012109 (2015).
- [26] S. Dutton, M. Kumar, M. Mourigal, Z. Soos, J.-J. Wen, C. Broholm, N. Andersen, Q. Huang, M. Zbiri, R. Toft-Petersen, and R. J. Cava, “Quantum Spin Liquid in Frustrated One-Dimensional LiCuSbO_4 ,” *Phys. Rev. Lett.* **108**, 187206 (2012).
- [27] In our previous work devoted to edge-shared chain cuprates we have used a more physical notation like LiSbCuO_4 with the effective magnetically inactive cation LiSb^{6+} followed by the magnetically active effective anion $(\text{CuO}_4)^{-6}$ as compared to the traditional chemical notation LiCuSbO_4 with increasing ionicity of the cations.
- [28] S.-L. Drechsler, O. Volkova, A. Vasiliev, N. Tristan, J. Richter, M. Schmitt, H. Rosner, J. Málek, R. Klingeler, A. Zvyagin, and B. Büchner, “The route of frustrated cuprates from antiferromagnetic to ferromagnetic spin-1/2 Heisenberg chains: $\text{Li}_2\text{ZrCuO}_4$ as a missing link near the quantum critical point,” *Phys. Rev. Lett.* **98**, 077202 (2007).
- [29] E. Vavilova, A. S. Moskvina, Y. C. Arango, S.-L. D. A. Sotnikov, R. Klingeler, O. Volkova, A. Vasiliev, V. Kataev, and B. Büchner, “Quantum electric dipole glass and frustrated magnetism near a critical point in $\text{Li}_2\text{ZrCuO}_4$,” *EPL* **88**, 27001 (2009).
- [30] R. B. Griffiths, “Magnetization curve at zero temperature for the antiferromagnetic Heisenberg linear chain,” *Phys. Rev.* **133**, A768 (1964).
- [31] Linarite and some other anisotropic CuO_2 chain systems with a low crystallographic symmetry [65] show the similar feature but at inconvenient for experimental studies higher fields above 30 T in the latter case.
- [32] C. P. Poole, *Electron Spin Resonance: A Comprehensive Treatise on Experimental Techniques* (Dover Publications, Mineola, NY, 1996).
- [33] A. Abragam and B. Bleaney, *Electron paramagnetic resonance of transition ions* (Clarendon Press, Oxford, 1970).
- [34] T. Moriya, “Nuclear magnetic relaxation in antiferromagnetics,” *Prog. Theor. Phys.* **16**, 23 (1956).
- [35] R. Chitra and T. Giamarchi, “Critical properties of gapped spin-chains and ladders in a magnetic field,” *Phys. Rev. B* **55**, 5816–5826 (1997).
- [36] M. Sato, T. Momoi, and A. Furusaki, “NMR relaxation rate and dynamical structure factors in nematic and multipolar liquids of frustrated spin chains under magnetic

- fields,” *Phys. Rev. B* **79**, 060406(R) (2009).
- [37] M. Sato, T. Hikihara, and T. Momoi, “Field and temperature dependence of NMR relaxation rate in the magnetic quadrupolar liquid phase of spin-1/2 frustrated ferromagnetic chains,” *Phys. Rev. B* **83**, 064405 (2011).
- [38] M. Greger, M. Kollar, and D. Vollhardt, “Isosbestic points: How a narrow crossing region of curves determines their leading parameter dependence,” *Phys. Rev. B* **87**, 195140 (2013).
- [39] M. Oshikawa and I. Affleck, “Field-induced gap in $s=1/2$ antiferromagnetic chains,” *Phys. Rev. Lett.* **79**, 2883 (1997).
- [40] M. Oshikawa and I. Affleck, “Low-temperature electron spin resonance theory for half-integer spin antiferromagnetic chains,” *Phys. Rev. Lett.* **82**, 5136 (1999).
- [41] M. Oshikawa and I. Affleck, “Electron spin resonance in $s=1/2$ antiferromagnetic chains,” *Phys. Rev. B* **65**, 134410 (2002).
- [42] K. Y. Povarov, A. I. Smirnov, O. A. Starykh, S. V. Petrov, and A. Y. Shapiro, “Modes of magnetic resonance in the spin-liquid phase of Cs_2CuCl_4 ,” *Phys. Rev. Lett.* **107**, 173 (2011).
- [43] A. I. Smirnov, T. A. Soldatov, K. Y. Povarov, and A. Y. Shapiro, “High-field magnetic resonance of spinons and magnons in the triangular lattice $s = 1/2$ antiferromagnet Cs_2CuCl_4 ,” *Phys. Rev. B* **91**, 174412 (2015).
- [44] H. Kühne, private communication, unpublished. (2016).
- [45] A. V. Syromyatnikov, “Spin nematic phase in one-dimensional and quasi-one-dimensional frustrated magnets in a strong magnetic field,” *Phys. Rev. B* **86**, 014423 (2012).
- [46] J. Málek, S.-L. Drechsler, U. Nitzsche, H. Rosner, and H. Eschrig, “Temperature dependent optical conductivity of undoped cuprates with weak exchange,” *Phys. Rev. B* **78**, 165118 (2008).
- [47] M. Monney and *et al.*, “Probing inter- and intrachain zhang-ricc excitons in Li_2CuO_2 and determining their binding energy interaction and weak ferromagnetism,” *Phys. Rev. B* **94**, 165118 (2016).
- [48] K. Rule, B. Willenberg, M. Schäpers, A. Wolter, S.-L. Drechsler, G. Ehlers, D. Tennant, R. Mole, J. Gardner, S. Süllow, and S. Nishimoto, “The dynamics of linarite: observation of magnetic excitations,” arXiv: , 1611.00986v2 (2016).
- [49] A. Bogdanov, U. Röfler, M. Wolf, and K. Müller, “Magnetic structures and reorientation transitions in noncentrosymmetric uniaxial antiferromagnets,” *Phys. Rev. B* **66**, 214410 (2002).
- [50] The present single chain Hamiltonian with the involved specific exchange anisotropy describes a 1D system with a distinctive nematically *ordered* ground state at $T = 0$ and at high enough magnetic fields in contrast with simple AFM Heisenberg chains. With increasing finite T this distinct order is more and more suppressed. The stability of the former generalized also to 2D or 3D with respect to interchain couplings and various DM couplings will be investigated in detail in forthcoming work.
- [51] Y. Katayama, T. Mizutani, W. Utsumi, O. Shimomura, M. Yamakata, and K.-I. Funokosho, “A first order liquid-liquid phase transition in phosphorus,” *Nature* **403**, 170 (2000).
- [52] R. Kurita and H. Tanaka, “Critical-like phenomena associated with liquid-liquid transition in a molecular liquid,” *Science* **306**, 845 (2004).
- [53] H. Tanaka, “Importance of many-body orientational correlations in the physical description of liquids,” *Faraday Discuss.* **167**, 9 (2013).
- [54] J. Rodríguez-Carvajal, “Recent advances in magnetic structure determination by neutron powder diffraction,” *Physica B: Condensed Matter* **192**, 55 – 690 (1993).
- [55] H. Nojiri, Y. Ajiro, T. Asano, and J.-P. Boucher, “Magnetic excitation of $s = 1/2$ antiferromagnetic spin chain Cu benzoate in high magnetic fields,” *New J. Phys.* **8**, 218 (2006).
- [56] C. Golze, A. Alfonsov, R. Klingeler, B. Büchner, V. Kataev, C. Mennerich, H.-H. Klauss, M. Goiran, J.-M. Broto, H. Rakoto, and et al., “Tuning the magnetic ground state of a tetranuclear Nickel(II) molecular complex by high magnetic fields,” *Phys. Rev. B* **73**, 224403 (2006).
- [57] H. Nojiri, T. Taniguchi, Y. Ajiro, A. Müller, and B. Barbara, “Quantum dynamics of molecular magnets in ultrafast sweeping magnetic fields,” *Physica B* **246-247**, 216 (2004).
- [58] K. Koepnik and H. Eschrig, “Full-potential nonorthogonal local-orbital minimum-basis band-structure scheme,” *Phys. Rev. B* **59**, 1743 (1999).
- [59] I. Ophale, K. Koepnik, and H. Eschrig, “Full-potential band-structure calculation of iron pyrite,” *Phys. Rev. B* **60**, 14035 (1999).
- [60] <http://www.fplo.de>.
- [61] J. Perdew and Y. Wang, “Accurate and simple analytic representation of the electron-gas correlation energy,” *Phys. Rev. B* **45**, 13244 (1992).
- [62] J. Perdew, K. Burke, and M. Ernzerhof, “Generalized gradient approximation made simple,” *Phys. Rev. Lett.* **77**, 3865 (1996).
- [63] M. Schmitt, J. Málek, S.-L. Drechsler, and H. Rosner, “Electronic structure and magnetic properties of $\text{Li}_2\text{ZrCuO}_4$: A spin- $\frac{1}{2}$ Heisenberg system close to a quantum critical point,” *Phys. Rev. B* **80**, 205111 (2009).
- [64] M. Mourigal, M. Enderle, B. Fak, R. Kremer, J. Law, A. Schneidewind, A. Hiess, and A. Prokofiev, “Evidence of a bond-nematic phase in LiCuVO_4 ,” *Phys. Rev. Lett.* **109**, 027203 (2012).
- [65] M. Hase, H. Kuroe, K. Ozawa, O. Suzuki, H. Kitazawa, G. Kido, and T. Sekine, “Confirmation of a one-dimensional spin-1/2 heisenberg system with ferromagnetic first-nearest-neighbor and antiferromagnetic second-nearest-neighbor interactions in $\text{rb}_2\text{cu}_2\text{mo}_3\text{o}_{12}$,” *Phys. Rev. B* **70**, 104426 (2004).
- [66] M. Hase, I. Terasaki, and K. Uchinokura, “Observation of the spin-peierls transition in linear Cu^{2+} (spin-1/2) chains in an inorganic compound CuGeO_3 ,” *Phys. Rev. Lett.* **70**, 3651–3654 (1993).
- [67] C. Agripidis, S.-L. Drechsler, J. van den Brink, and S. Nishimoto, “Cross-over from an incommensurate singlet spiral state with an exponentially small spin-gap to a valence bond solid state in dimerized frustrated ferromagnetic spin-chains,” arXiv: , 1612.07609v1 (2016).
- [68] S. Meiboom, J. Sethna, P. Anderson, and W. Brinkman, “Theory of the blue phase of cholesteric liquid crystals,” *Phys. Rev. Lett.* **46**, 1216 (1981).
- [69] H. Wilhelm, M. Baenitz, M. Schmidt, C. Naylor, R. Lortz, U. Röfler, A. Leonov, and A. Bogdanov, “Confinement of chiral magnetic modulations in the precursor region of FeGe ,” *J. Phys.: Condens. Matter* **24**, 294204 (2012).

- [70] J. Toledano and P. Toledano, *The Landau theory of phase transitions* (World Scientific, 1987).
- [71] M. Yamashita, “First order phase transition accompanying soliton lattices near a tricritical point - chiral smectic c liquid crystal in an electric field -,” *J. Phys. Soc. Jpn.* **56**, 1414 (1987).
- [72] B. Schaub and D. Mukamel, “Phase diagrams of systems exhibiting incommensurate structures,” *Phys. Rev. B* **32**, 6385 (1985).
- [73] C. Kegler, N. Büttgen, H.-A. Krug von Nidda, and A. Loidl, “NMR study of lineshifts and relaxation rates of the one-dimensional antiferromagnet LiCuVO_4 ,” *Phys. Rev. B* **73**, 104418 (2006).
- [74] A. Smerald and N. Shannon, “Angle-resolved nmr: Quantitative theory of ^{75}As T_1 relaxation rate in bafe_2as_2 ,” *Phys. Rev. B* **84**, 184437 (2011).

Supplement

Details of the exchange and kinematic interactions as derived from the band structure calculations The two tiny third neighbor interactions $J_3 \sim 1.6$ to 3.2 K, respectively, were both ignored in the DMRG calculations for the sake of simplicity, i.e. first of all to restrict the number of model parameters. Note that the NN exchange integrals may have a margin of error about a few ten K due to several uncertainties like in U_{eff} and a more accurate estimation is left for future work. However, the alternation of the NN exchange integrals is most likely, a rare situation so far only met for the celebrated spin-Peierls compound CuGeO_3 [66] with two AFM NN couplings and probably with two ferromagnetic ones for $\text{Rb}_2\text{Cu}_2\text{Mo}_3\text{O}_{12}$ [65, 67], only. The interchain transfer integrals were derived employing the calculated Wannier functions to reproduce the full DFT band dispersion of the band complex near the Fermi energy. Their overlapping tails are smaller by an order of magnitude ~ 10 meV as compared to the NN inchain values giving this way rise to still smaller frustrated AFM contributions of the order of 1 K, only, (Fig. 1). Since there are no reasons to expect significant FM contributions the resulting total interchain couplings are expected to be extremely small, too. This qualitative estimate might explain the strongly suppressed SDW and spiral phases and most importantly will only weakly suppress the nematic state [24].

Detailed symmetry analysis: Non-centrosymmetric crystal structure from the class C_{2v} : generalities The crystal structure of LiCuSbO_4 has been described in the acentric (polar) space-group $\text{Cmc}2_1$ (No 36, point symmetry C_{2v}) [26]. The low symmetry allows that DM interactions,

$$E_D = \mathbf{D}_{ij} \cdot (\mathbf{S}_i \times \mathbf{S}_j), \quad (6)$$

can occur for *all* bonds between two Cu-sites. A long-range-ordered magnetic state (or the hypothetical mean-field magnetic order) in these materials may appear as a basically AFM spin-pattern that is twisted into long-period textures. A 1D texture is known as a "Dzyaloshinskii spiral". A monodomain-state of such a spiral has a spatially fixed rotation axis w.r.t. to its propagation direction and a fixed (chiral) sense of rotation. In the crystal classes C_{nv} , $n = 2, 3, 4, 6$ the possible propagation directions \mathbf{p} are perpendicular to the unique axis of the crystals \mathbf{c} . The propagation direction in the ground-state is determined by weaker anisotropies of the magnetic system. The rotation axis for the spins is transverse to this propagation axis and also is in the plane perpendicular to the crystallographic axis. Thus, the staggered vector rotates in a cycloidal manner within the plane spanned by the propagation direction \mathbf{p} and the axis c . This slow rotation of the primary order-parameter components is accompanied by a (weak-FM) spin-density wave, similar to magnets from crystal classes (C_{nv} , $n = 3, 4, 6$) anal-

ysed in Ref. 49.

In general, Lifshitz invariants in several spatial directions do *frustrate* long-range ordering (LRO) as these terms act like a frozen gauge potential background on the incipient ordering and enhances the impact of fluctuations to destroy LRO as has been described for a wide range of different systems from cholesteric liquid crystals [68] to chiral magnets [69]. In a paramagnetic but spin-liquid state of an AFM system with C_{2v} symmetry, a possible kind of correlated low-energy excitations would consist of skyrmionic modes. These are localized excitations (possibly in the shape of ellipsoidal staggered spin-states) that are twisted in the two basal plane directions. Other possible excitation modes would be 1D kink-like solitonic units with an envelope function of the order-parameter that restricts their spatial extension on a paramagnetic background.

In both kinds of such non-linear excitations, the magnitude and direction of the AFM correlations within such a fluctuating excitation are intertwined and cannot be separated [69–72]. For a fully established 3D spin-order, the Lifshitz-type invariants for the vector components of a magnetic ordering mode have spatial gradients in the base-plane (perpendicular to the n -fold crystal axis) in the continuum theory for crystals from the classes C_{nv} . The very existence of strong enough frustrating DMIs will tend to suppress classical 3D long-range ordering and exacerbate the impact of quantum-fluctuations in a low-dimensional spin-system.

Experimental details NMR

Experimental determination of the hyperfine coupling: Fig. 11 shows the Knight shift K determined from the peak of the spectra in 3 T and 15 T versus the macroscopic susceptibility χ of the powder sample in 3 T. Linear fits give hyperfine coupling constants of $A_{hyp} \approx -0.27 \text{ kOe}/\mu_B$, and an orbital shift of $K_{orb} = -0.005\%$ for 3 T and $A_{hyp} \approx -0.24 \text{ kOe}/\mu_B$, and $K_{orb} = -0.002\%$ for 15 T. This is comparable to the value extracted in LiCuVO_4 for a field perpendicular to the chain direction, $A_{perp} = -0.19 \text{ kOe}/\mu_B$ [73]. Anisotropic hyperfine coupling as can be determined by measurements on single crystals (see, e.g., [19, 74]) cannot be extracted since only powder susceptibility data are available.

Calculation of the hyperfine tensor: The local field of the Cu electron spins \mathbf{S}_j at the nuclear spin \mathbf{I}_i of the Li $\mathbf{h}_i = \sum_j \hat{A}_{ij} \langle \mathbf{S}_j \rangle$ is transferred by the dipolar hyperfine coupling tensor

$$\hat{A}_i = \sum_j \hat{A}_{ij} = \begin{pmatrix} A_i^{aa} & A_i^{ab} & A_i^{ac} \\ A_i^{ba} & A_i^{bb} & A_i^{bc} \\ A_i^{ca} & A_i^{cb} & A_i^{cc} \end{pmatrix} \quad (7)$$

where a , b and c denote the crystallographic axes. In the paramagnetic state h_i is proportional to χ , since $\langle \mathbf{S} \rangle \sim \chi \mathbf{H}$. Compared to the case of LiCuVO_4 where the tensor Eq. (7) was determined by Nawa *et al.* [19] by measurements on single crystals, LiCuSbO_4 is only available as powder samples. In addition, there are two

different Li sites in LiCuSbO_4 (Fig. 1). Li(1) is coupled most strongly to six Cu spins in three nearest neighboring chains, and Li(2) is coupled to four Cu spins in two nearest neighboring chains. The dipolar hyperfine coupling tensors for both Li sites have been calculated by lattice sum over a radius of 160 \AA and are given in units $[\text{kOe}/\mu_B]$:

$$\hat{A}_1 = \begin{pmatrix} -0.21 & 0.13 & -0.0005 \\ 0.13 & 0.27 & -1.0 \\ -0.0005 & -1.0 & -0.061 \end{pmatrix} \quad (8)$$

$$\hat{A}_2 = \begin{pmatrix} -0.29 & 0.014 & 0.015 \\ 0.014 & -0.18 & -1.02 \\ 0.015 & -1.02 & 0.474 \end{pmatrix} \quad (9)$$

For both Li sites, there are diagonal elements which agree with the hyperfine coupling determined from the K vs. χ plot in Fig.11. This means, the main peak in the spectrum contains intensity of both Li sites. Note, that also the off-diagonal elements may contribute to the main peak due to the powder averaging of a specific angular dependence of h_i , and that a small transferred hyperfine coupling may exist, too.

The off-diagonal elements can transfer longitudinal electron spin fluctuations in the paramagnetic state to transverse fluctuating hyperfine fields at the Li site (cf. Eq. (1) in the main text). This would lead to spin lattice relaxation by longitudinal spin fluctuations. On the other hand, if spin correlations are peaked for certain wave vectors \mathbf{Q}_0 in the short-range ordered helical, SDW or nematic states, phase factors $\Theta(\mathbf{q})$ may lead to a cancellation of these off-diagonal elements making T_1^{-1} insensitive to longitudinal spin fluctuations [19]. However, such a sharp peak at \mathbf{Q}_0 is expected only for the field in the chain direction and not perpendicular to it due to the weak intra-chain coupling [19]. Thus, in the measurements on a powder sample of LiCuSbO_4 where all orientations contribute to the NMR signal one can reasonably expect that both longitudinal and transverse spin fluctuations give rise to the spin lattice relaxation at all temperatures.

Spin lattice relaxation, fits and stretched exponential relaxation: Fig.12 shows three exemplary fits of the nuclear magnetization M versus time τ for a magnetic field of 16 T at 20K, 4.2K, and 1.7 K. $M(\tau)$ could then be fitted to a single exponential function $M(\tau) = M_0\{1 - f \exp[-(\tau/T_1)^b]\}$ with $f = 1$ for ideal saturation. At 4.2 K, two fits are shown: one with a fixed stretching exponent $b = 1$, and one with b as a free fitting parameter ($b = 0.81$). The difference is negligible and the extracted T_1 value is the same within the error bars. Only at the lowest temperatures a stretching exponent is necessary to fit the data, as can be seen for the data measured at 1.7K. The lower panel of Fig. 12 shows the stretching exponent b for all fields and temperatures below 20K. Only at higher fields $> 13 \text{ T}$ and very low T a substantial distribution of spin lattice relaxation rates appears.

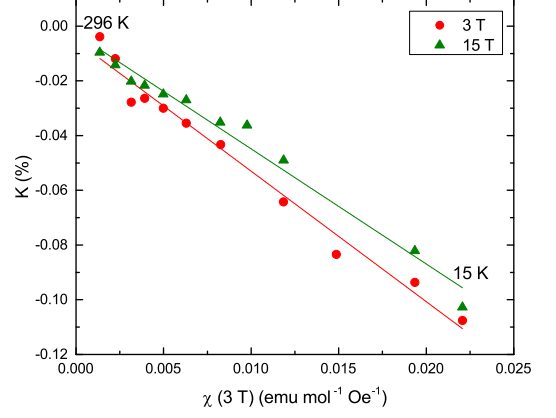


FIG. 11. Knight shift determined in 3 and 15 T versus macroscopic susceptibility of the powder sample in 3 T. The lines are fits as described in the main text.

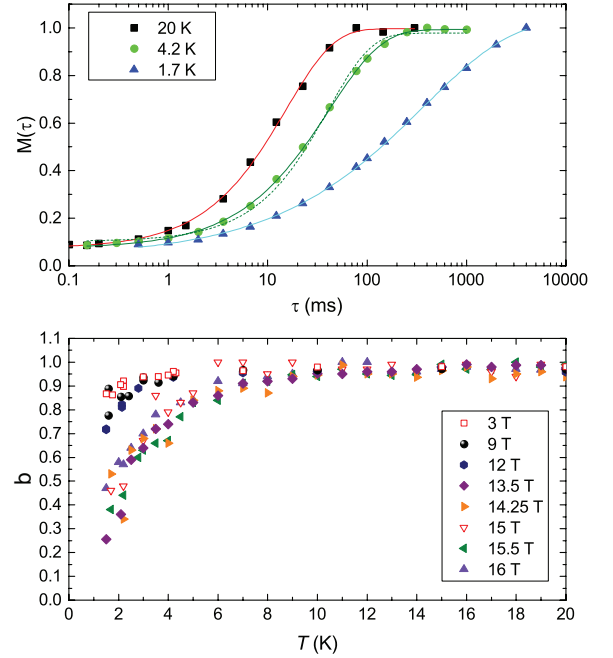


FIG. 12. Upper panel: Nuclear magnetization M versus τ in 16 T and for three different temperatures. The lines are fits as described in the text. The dashed line is a fit with b fixed to 1. Lower panel: Stretching exponent b versus temperature for all different fields.

Modelling of the $T_1^{-1}(T)$ dependences: Experimental $T_1^{-1}(T)$ curves for all measured magnetic fields (Fig. 5) were modelled with Eq. (3). The fit parameters are presented in Fig. 13.

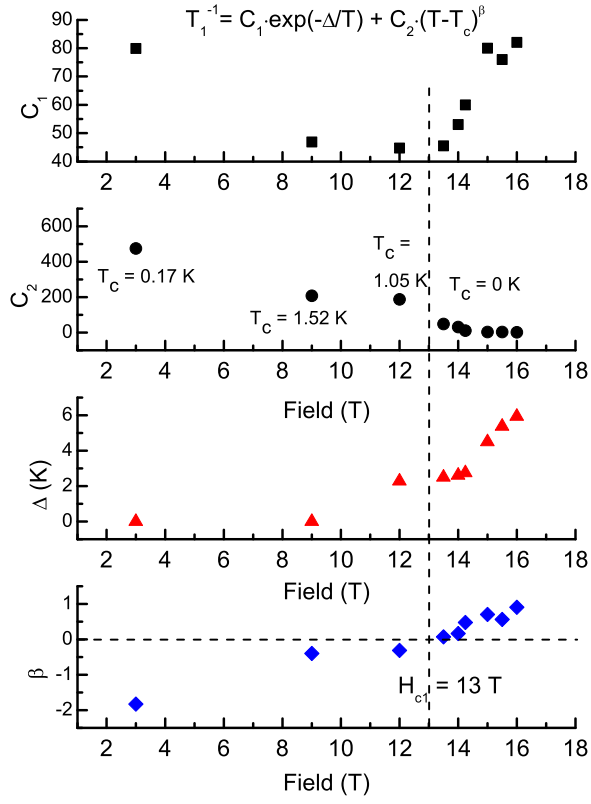


FIG. 13. Magnetic field dependence of the model parameters according to Eq. (3). Vertical dashed line denotes the critical field $H_{c1} = 13$ T corresponding to the isosbestic point in Fig. 6.